DOI: 10.1002/((please add manuscript number))

Article type: Full Paper

Effect of the Selective Halogenation of Small Molecule Acceptors on the Blend Morphology and Voltage Loss of High-Performance Solar Cells

Geon-U Kim[†,a], Cheng Sun[†,b], Dongchan Lee[†,c], Gi-Seok Choi[†, a], Jin Su Park[a], Soodeok Seo[a], Seungjin Lee[a], Do-Yeong Choi [d], Soon-Ki Kwon [d], Shinuk Cho [c,], Yun-Hi Kim [b,*], and Bumjoon J. Kim [a,*]*

[a] G.-U Kim, G.-S. Choi, J. S. Park, S. Seo, S. Lee, Prof. B. J. Kim

Department of Chemical and Biomolecular Engineering, Korea Advanced Institute of Science and Technology (KAIST), Daejeon 34141, Republic of Korea

E-mail: bumjoonkim@kaist.ac.kr

[b] C. Sun, Prof. Y.-H. Kim

Department of Chemistry and RIGET, Gyeongsang National University, Jinju 52828, Republic of Korea

E-mail: ykim@gnu.ac.kr

[c] D. Lee, Prof. S. Cho

Department of Physics and EHSRC, University of Ulsan, Ulsan 44610, Republic of Korea

E-mail: sucho@ulsan.ac.kr

[d] D.-Y. Choi, Prof. S.-K. Kwon

Department of Materials Engineering and Convergence Technology and ERI, Gyeongsang National University, Jinju 52828, Republic of Korea

Keywords: organic solar cells, small molecule acceptors, halogenation, blend morphology, voltage loss

Abstract

Herein, we describe the impacts of the selective halogenation at two different positions of dicyanomethylene-3-indanone (IC)-end groups and inner side-chains of SMAs on the P_D:SMA interfacial interactions, blend morphology, and resulting photovoltaic properties. In this study, four different SMAs (A1, A2, A3, and A4) with the same molecular backbone, but with different degrees of halogenation, are synthesized. The IC-end groups on the backbones of the A1 and A3, and A2 and A4 SMAs are chlorinated and fluorinated, respectively; in addition, 6-phenoxyhexyl inner side-chains of the A3 and A4 are chlorinated. The SMAs are paired with a chlorinated PBDT-Cl P_D to construct OSCs. The PBDT-Cl:A4-based OSC exhibits the highest PCE of 17.2%, outperforming the PBDT-Cl:A1- (13.3%), PBDT-Cl:A2-(15.6%), and PBDT-Cl:A3-based OSC (16.5%). The Cl atoms on the side-chains in the A3 and A4 SMAs enhance the molecular/energetic interactions at the P_D:SMA interfaces and improve the blend morphology in terms of domain purity and spacing. These effects lead to the improved fill factors and reduced voltage loss of the PBDT-Cl:A3- and PBDT-Cl:A4-based OSCs. Our

study demonstrates the importance of appropriate halogenation of SMAs in optimizing the blend morphology, reducing voltage loss, and improving OSC performance.

1. Introduction

Organic solar cells (OSCs) have the merits of semitransparency, cost effectiveness, light weight, mechanical durability, and solution processability.[1] The power conversion efficiencies (PCEs) of bulk heterojunction (BHJ) OSCs have remarkably increased to over 18%, which is mainly driven by the development of efficient polymer donors (P_Ds) and small molecular acceptors (SMAs) with excellent light-absorption ability and electrical properties.[2] To further improve the PCE over 20%, optimizing the pairing of P_Ds and SMAs is an important task.[3] Requirements such as (1) well-matched energy levels, (2) optimal blend morphology with favorable P_D/SMA interactions, and (3) reduced voltage loss (V_{loss}) should be considered when finding optimal P_D/SMA pairs.[4]

Most efficient SMAs, such as Y-families, have molecular structures of acceptor-donor-acceptor-donor-acceptor (A-DA'D-A) backbone.[2b, 3, 5] Owing to the availability of multiple positions suitable for chemical modification, significant effort has been directed at improving the properties of these SMAs.[6] Among the possible structural modifications of SMAs, halogenation, the introduction of electron-withdrawing halogen atoms (*i.e.*, fluorine (F) and chlorine (Cl)), is considered a simple yet effective strategy for modulating the characteristics of the SMAs, including light-absorption ability,

energy levels, molecular planarity, and intermolecular assembly.[7] In addition, secondary interactions (*i.e.*, F (or Cl)···S and F (or Cl)···H) induced by halogenation improve the inter- or intramolecular interactions and crystalline packing and, thus, enhance charge transport ability of the SMAs.[7e] Importantly, the halogenation of SMAs can significantly affect their molecular interactions and miscibility with P_Ds in blends, thus affecting the blend morphology and PCE of resulting OSCs. Recently, Marks *et al.* reported BT-BO-based SMA series with different numbers of F atoms in their 1,1-dicyanomethylene-3-indanone (IC)-end groups. The PCEs of the resulting OSCs were significantly increased with fluorination of the SMA from 9.6% (without F atoms) to 16.8% (with four F atoms).[8] He *et al.* developed BTIC-4Cl-T-based SMA series featuring conjugated thiophene rings in their outer side-chains with different chlorination patterns. The PCEs of the OSCs based on BTIC-4Cl-TCl-β with chlorinated side-chains (15.65%) considerably exceeded those of the OSCs based on BTIC-4Cl-T with non-chlorinated side-chains (10.86%).[6a] In our previous work, the use of both a fluorinated P_D (PBDT-F) and SMA (C6OB-F) achieved an OSC with a significantly higher PCE (15.21%) than that (10.06%) of an OSC based on a non-fluorinated P_D (PBDT-H) and fluorinated SMA (C6OB-F).[4f] These studies verify that the halogenation of the end groups or side-chains of P_Ds and SMAs significantly affects P_D/SMA interactions in blends, charge generation/recombination properties, and thus photovoltaic performances.

The V_{loss} is one of the most critical factors limiting the PCEs in the OSCs. In particular, the contribution from non-radiative V_{loss} should be reduced, which is mainly affected by the energetic interactions at the P_Ds/SMAs interfaces. Thus, the interfacial and morphological properties (*i.e.*, domain size/purity, aggregation, and molecular orientation) of the BHJ blend should be optimized to reduce the non-radiative V_{loss}.[9] For instance, Yan *et al.* investigated a blend system of PvBDTTAZ

P_D and O-IDTBR SMA, where the resulting OSC with a PCE of 11.6% showed a very low V_{loss} of 0.55 V and thus high open–circuit voltage (V_{oc}) of 1.08 V.[10] The key contributions to the low V_{loss} were both the high crystallinity and small domain sizes in the BHJ morphology. As another example, Nguyen *et al.* investigated the effect of the P_D packing orientation on the non-radiative V_{loss}. The OSC based on a face-on orientated p-SIDT(FBTTh$_2$)$_2$ P_D exhibited a lower non-radiative V_{loss}, and thus a higher V_{oc} (0.84 V), than the other OSC based on an edge-on orientated P_D (V_{oc} = 0.69 V).[11] Therefore, it is expected that the halogenation of SMAs can effectively reduce and increase the non-radiative V_{loss} and V_{oc}, respectively, of OSCs by improving the molecular interaction and energetic order between P_Ds and SMAs at their interfaces.

In this work, we investigate the impact of the halogenation of SMAs on their molecular properties, P_D/SMA interactions, blend morphology, and the V_{loss} and PCE of the resulting OSCs. Four different SMAs with the same backbone, but with different degrees of halogenation are designed and synthesized (**Figure 1**). The four SMAs, 2,2′-((2Z,2′Z)-((12,13-bis(6-phenoxyhexyl)-3,9-diundecyl-12,13-dihydro-[1,2,5]thiadiazolo[3,4-*e*]thieno[2″,3″:4′,5′]thieno[2′,3′:4,5]pyrrolo[3,2-*g*]thieno[2′,3′:4,5]thieno[3,2-*b*]indole-2,10-diyl)bis(methanylylidene))bis(5,6-dichloro-3-oxo-2,3-dihydro-1*H*-indene-2,1-diylidene))dimalononitrile (SMA-Cl-H), 2,2′-((2Z,2′Z)-((12,13-bis(6-phenoxyhexyl)-3,9-diundecyl-12,13-dihydro-[1,2,5]thiadiazolo[3,4-

e]thieno[2′′,3′′:4′,5′]thieno[2′,3′:4,5]pyrrolo[3,2-*g*]thieno[2′,3′:4,5]thieno[3,2-*b*]indole-2,10-diyl)bis(methanylylidene))bis(5,6-difluoro-3-oxo-2,3-dihydro-1*H*-indene-2,1-diylidene))dimalononitrile (SMA-F-H), 2,2′-((2Z,2′Z)-((12,13-bis(6-(3-chlorophenoxy)hexyl)-3,9-diundecyl-12,13-dihydro-[1,2,5]thiadiazolo[3,4-*e*]thieno[2′′,3′′:4′,5′]thieno[2′,3′:4,5]pyrrolo[3,2-*g*]thieno[2′,3′:4,5]thieno[3,2-*b*]indole-2,10-diyl)bis(methanylylidene))bis(5,6-dichloro-3-oxo-2,3-dihydro-1*H*-indene-2,1-diylidene))dimalononitrile (SMA-Cl-Cl), and 2,2′-((2Z,2′Z)-((12,13-bis(6-(3-chlorophenoxy)hexyl)-3,9-diundecyl-12,13-dihydro-[1,2,5]thiadiazolo[3,4-*e*]thieno[2′′,3′′:4′,5′]thieno[2′,3′:4,5]pyrrolo[3,2-*g*]thieno[2′,3′:4,5]thieno[3,2-*b*]indole-2,10-diyl)bis(methanylylidene))bis(5,6-difluoro-3-oxo-2,3-dihydro-1*H*-indene-2,1-diylidene))dimalononitrile, (SMA-F-Cl), are denoted by A1, A2, A3, and A4, respectively. First, we introduce halogen atoms at the IC-end groups, where A1 and A3 have Cl atoms and A2 and A4 have F atoms. Furthermore, Cl atoms are incorporated into the terminal benzene rings of the 6-phenoxyhexyl side-chains of the A3 and A4 SMAs.[7c] Among OSCs based on these SMAs and a PBDT-Cl P_D, the PBDT-Cl:A4-based OSC achieves the

highest PCE of 17.19% (V_{oc} = 0.840 V, short–circuit current (J_{sc}) = 26.90 mA cm^{-2}, and fill factor (FF) = 0.76), outperforming the PBDT-Cl:A1-, PBDT-Cl:A2, and PBDT-Cl:A3-based OSC with PCEs of 13.33, 15.59, and 16.55%, respectively. These results demonstrate the importance of the selective halogenation on the IC-end groups and inner side-chains of SMAs in enhancing photovoltaic performance. Notably, the chlorination of the side-chains in the A3 and A4 SMAs induces the favorable molecular packing structures and increases the energetic interactions at the P_D/SMA interfaces, reducing the non-radiative V_{loss} of corresponding OSCs. In particular, the PBDT-Cl:A3-based blend film shows a favorable face-on packing orientation and the corresponding OSC exhibits a much lower non-radiative V_{loss} (0.278 V) than the PBDT-Cl:A1-based OSC (0.352 V), whose blend film shows mixed edge-on/face-on packing orientations. The morphological properties of the blends are thoroughly investigated by the grazing-incidence X-ray scattering (GIXS) and resonant soft X-ray scattering (RSoXS) measurements.

2. Results and Discussion

2.1. Design Strategy and Material Properties

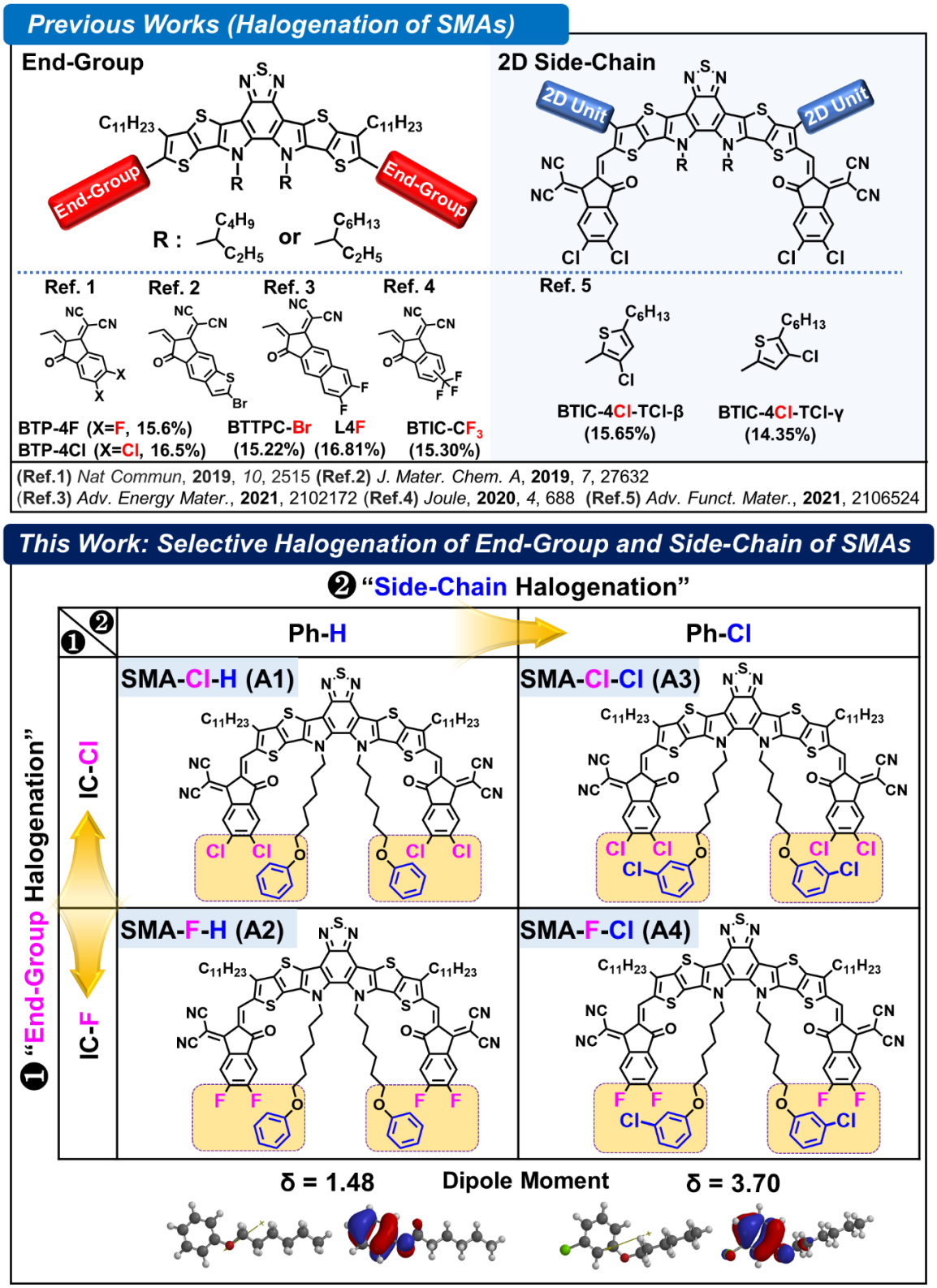

Figure 1. Material design of the SMAs investigated in this work.

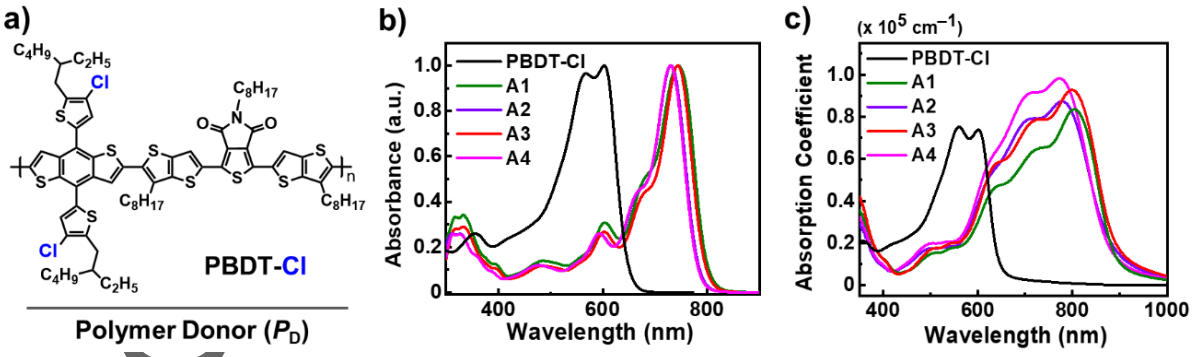

Figure 2. a) Molecular structure of the P_D used in this study. b) UV-Vis absorption spectra in dilute chloroform solutions and c) UV-Vis absorption spectra in chloroform-processed thin films of the SMAs and PBDT-Cl P_D.

Table 1. Optical/electrochemical characteristics of the four SMAs and PBDT-Cl P_D.

Material	λ_{sol}^{max} [nm]	λ_{film}^{max} [nm]	$\lambda_{film,TA}^{max}$ [nm]	$\varepsilon_{film,CF}$ [× 10^4 cm^{-1}]	E_g^{opt} a) [eV]	E_{HOMO} b) [eV]	E_{LUMO} c) [eV]
PBDT-Cl	568, 603	559, 601	560, 601	7.52	1.89	–5.53	–3.64
A1	744	805	816	8.35	1.38	–5.67	–4.29
A2	731	778	822	8.73	1.38	–5.68	–4.30
A3	744	802	841	9.27	1.38	–5.69	–4.31

A4	730	773	824	9.82	1.39	–5.65	–4.26

[a] from the absorption onset wavelengths of the thin films. [b] from corresponding cyclic voltammetry. [c] $E_{LUMO} = E_g^{opt} + E_{HOMO}$.

The introduction of electron-withdrawing halogen atoms into the main backbones of SMAs (*i.e.*, IC end-groups) has been considered an effective strategy for modulating the light-absorption ability, energy level, molecular packing, and crystallization behaviors of the SMAs (**Figure 1**).[7] However, the significance of the halogenation on the terminal groups of non-conjugated side-chains has been relatively overlooked. Without compromising the electronic properties of SMAs, this strategy can effectively modulate the molecular compatibility and energetical interaction between P_D and SMA because the terminal units of the side-chains have the closest interactions with P_D at D/A interfaces.[4f] In this study, to systematically investigate the synergetic effects of the selective halogenation on the IC end-groups and non-conjugated side-chains of SMAs on photovoltaic performance, four different SMA-Xs (terminal units of IC end-

group)-Ys (terminal units of side-chain) (*i.e.*, SMA-Cl-H (A1), SMA-F-H (A2), SMA-Cl-Cl (A3), and SMA-F-Cl (A4)) are designed and synthesized (**Figure 1**). The IC end-groups of the A1 and A3 SMAs are chlorinated (denoted by IC-Cl), while those of A2 and A4 SMA are fluorinated (denoted by IC-F). In addition, the A1 and A2 SMAs have non-halogenated 6-phenoxyhexyl inner side-chains (denoted by Ph-H), while the A3 and A4 SMAs have Cl-attached 6-(3-chlorophenoxy)hexyl side-chains (denoted by Ph-Cl). Among the SMAs, the molecular structure of A2 SMA has been reported in the previous paper.[4f] The design rationale for the chlorination of the inner side-chains in the SMAs is that the Cl atoms with an empty 3d orbitals can readily accept π electrons, which may lead to strong non-covalent interactions such as Cl···π.[7c] Chlorination can also increase the dipole moment of the side-chains, which affects the intra- or intermolecular interactions of the SMAs.[7c] Indeed, the dipole moment (δ) of the Ph-Cl side-chain (δ = 3.70) exceeds that of the Ph-H side-chain (δ = 1.48), according to density functional theory (DFT) analysis (**Figure 1**). The synthetic procedures for the SMAs are presented in the Experimental Section, **Scheme S1,** and **Figures S1**–**S7**. To examine the solution-

processability of the SMAs, we estimated the solubilities of A1, A2, A3, and A4 in CF (**Figure S8**). All the SMAs showed reasonably high solubilities (> 20 mg mL^{-1}), regardless of the type of halogen atoms attached on the terminal units of side-chains and IC-end groups. This result indicates that 6-phenoxyhexyl inner side-chain is a good solubilizing group.

A PBDT-Cl P_D, comprising thienothiophene π-bridged *N*-octylthieno[3,4-*c*]pyrrole-4,6-dione (8ttTPD) and chloro-benzodithiophene (BDT-Cl) building blocks, is synthesized and paired with the SMAs.[12] The PBDT-Cl P_D and four SMAs have appropriate energy level alignment and complementary light absorption ranges (**Figure 2**).[4f, 12] The optical and electrochemical characteristics of the materials are presented in **Table 1**. The highest occupied molecular orbital (HOMO) and lowest unoccupied molecular orbital (LUMO) energy levels of the P_D and four SMAs were determined from the cyclic voltammetry (CV) (**Figure S9**). All the SMAs exhibit similar HOMO and LUMO energy levels ranging from –5.69 to –5.65 eV and –4.31 to –4.26 eV, respectively, owing to their similar halogenated IC end-groups. In UV-Vis absorption spectra of the SMAs in

thin-films (**Figure 2c**), the A1 and A3 SMAs featuring IC-Cl end-group exhibit more red-shifted maximum absorption peaks than A2 and A4 SMAs featuring IC-F end-groups due to their different intramolecular charge transfer (ICT) abilities.[13] The maximum absorption coefficients ($\varepsilon_{film,CF}$) of chloroform (CF)-processed A1, A2, A3, and A4 thin films are 8.35 × 10^4 cm^{-1}, 8.73 × 10^4 cm^{-1}, 9.27 × 10^4 cm^{-1}, and 9.82 × 10^4 cm^{-1}, respectively. These results indicate that the A3 and A4 SMAs featuring Ph-Cl inner side-chains can harvest more photons than A1 and A2 SMAs featuring Ph-H inner side-chains. The thermal property of the SMAs was investigated from the thermogravimetric analysis (TGA). The thermal decomposition temperatures of the four SMAs were similar in the range of 315–320 °C, indicating a good thermal stability (**Figure S10**).

The electron mobilities (μ_es) of the CF-processed thin films of the pristine SMAs were obtained using the space-charge limited current (SCLC) method (**Table S1**).[14] Interestingly, the μ_es of SMAs featuring IC-F end-groups, A2 (5.2 × 10^{-4} cm^2 V^{-1} s^{-1}) and A4 (6.6 × 10^{-4} cm^2 V^{-1} s^{-1}), exceed those of SMAs featuring IC-Cl end-group, A1 (2.7 × 10^{-4} cm^2 V^{-1} s^{-1}) and A3 (3.8 × 10^{-4} cm^2 V^{-1} s^{-1}). More importantly, owing to the

chlorination of their inner side-chains, the μ_es of A3 and A4 SMAs outperform those of the A1 and A2 SMAs, respectively. Differential scanning calorimetry (DSC) measurement was conducted to understand the correlation between the SCLC mobilities and the crystalline properties of the SMAs. The SMA samples for DSC were prepared in the same conditions as SCLC measurement.[15] As shown in **Figure S11**, A2 and A4 SMAs featuring IC-F end-groups show distinct peaks in their first heating curves. The melting temperatures (T_m) and melting enthalpy (ΔH_m) of A2 SMA are 275°C and 24.5 J g^{-1} (**Table S2**). In the case of A4 SMA, two peaks at 255 and 272°C correspond to ΔH_ms of 10.8 and 17.2 J g^{-1}, respectively, thus the sum of ΔH_ms (28.0 J g^{-1}) of A4 SMA exceeds the ΔH_m of A2 SMA. On the other hand, A1 and A3 SMAs featuring IC-Cl end-groups show no obvious peaks. These results indicate that the SMAs having IC-F end-groups exhibit more enhanced molecular ordering and thin-film crystallinity than SMAs having IC-Cl end-groups. This trend is consistent well with that observed in the μ_es of the SMAs.

2.2. Photovoltaic Properties of the Blend Films

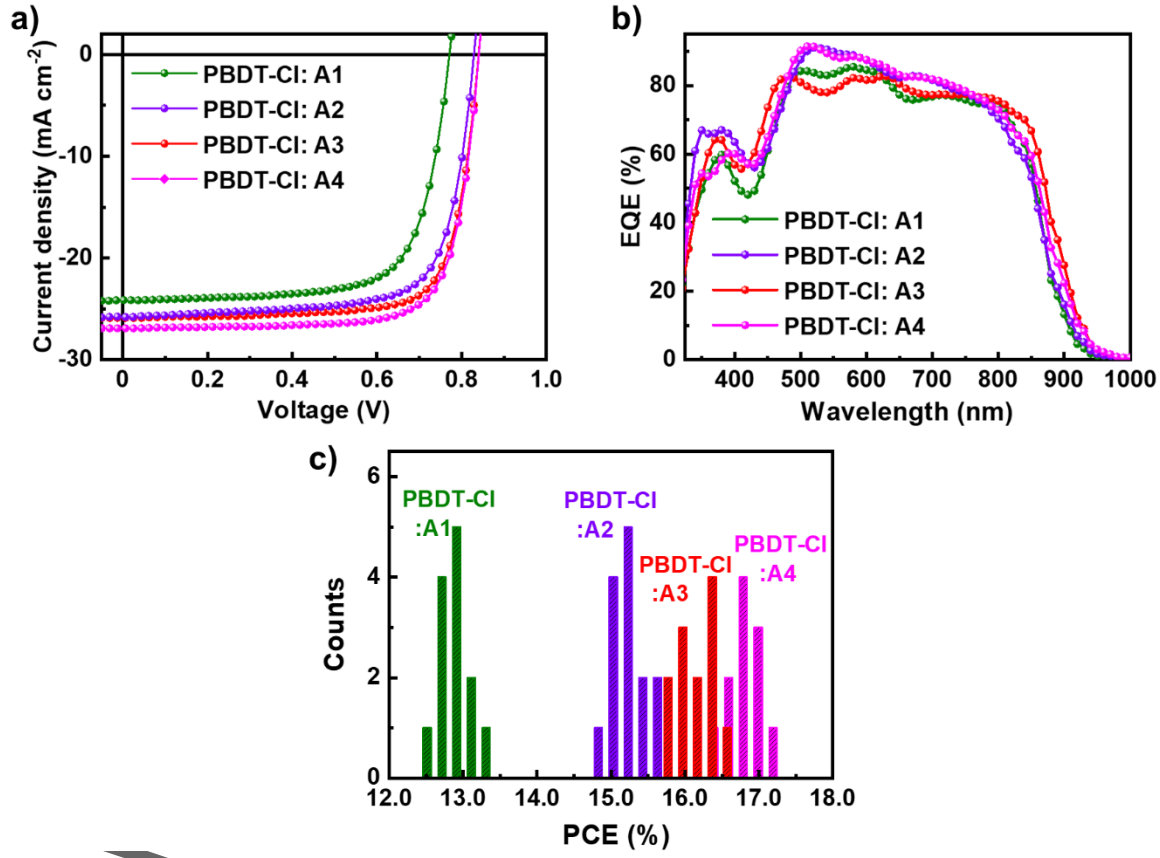

Figure 3. a) *J–V* curves, b) EQE curves, and c) PCE distributions of PBDT-Cl:AX (X= 1, 2, 3, or 4)-based OSCs.

Table 2. Photovoltaic performances of PBDT-Cl:AX (X= 1, 2, 3, or 4)-based OSCs.

P_D	SMAs	V_{oc} [V]	J_{sc} [mA cm^{-2}]	Calcd. J_{sc} [a)] [mA cm^{-2}]	FF	PCE_{max} (PCE_{avg}) [b)] [%]

PBDT-Cl	A1	0.771 (0.766 ± 0.004)	24.13 (23.83 ± 0.28)	24.12	0.71 (0.71 ± 0.01)	13.33 (12.92 ± 0.41)
	A2	0.828 (0.826 ± 0.005)	25.79 (25.43 ± 0.35)	25.08	0.73 (0.73 ± 0.00)	15.59 (15.25 ± 0.34)
	A3	0.840 (0.838 ± 0.002)	25.88 (25.82 ± 0.19)	25.18	0.76 (0.75 ± 0.01)	16.55 (16.38 ± 0.17)
	A4	0.840 (0.835 ± 0.005)	26.90 (26.78 ± 0.12)	25.62	0.76 (0.75 ± 0.01)	17.19 (16.87 ± 0.32)

[a] Calculated from the corresponding EQE spectrum. [b] obtained from at least 10 OSCs based on each P_D:SMA pair.

To assess the photovoltaic performances of each blend film, normal-type OSCs (ITO/poly(3,4-ethylenedioxythiophene):poly(styrenesulfonate) (PEDOT:PSS)/active layers/2,9-bis(3-((3-(dimethylamino)propyl)amino)propyl)anthra[2,1,9-*def*:6,5,10-

d′*e*′*f*′]diisoquinoline-1,3,8,10(2*H*,9*H*)-tetraone (PDINN)/Ag) were fabricated.[16] The optimization process for the OSCs is presented in **Table S3**. The current density–voltage (*J*–*V*) curves, external quantum efficiency (EQE) spectrum, and PCE distributions of each device are shown in **Figure 3a**–**c**. In **Table 2,** the corresponding photovoltaic parameters (V_{oc}s, J_{sc}s, FFs, and PCEs) are summarized. Among the fabricated OSCs, the PBDT-Cl:A4-based OSC obtained the highest PCE of 17.19%, outperforming the PBDT-Cl:A2-based OSC (PCE= 15.59%). Similarly, the PBDT-Cl:A3-based OSC afforded a higher PCE of 16.55% than the PBDT-Cl:A1 counterpart (PCE= 13.33%), demonstrating the effectiveness of the chlorination on the inner side-chain of SMAs in enhancing photovoltaic performance. Interestingly, the V_{oc}s of P_D:SMA-based OSCs were greatly increased by introducing Cl atoms into the inner side-chains of SMAs, despite their similar LUMO energy levels. For instance, the V_{oc} of the PBDT-Cl:A4-based OSC (V_{oc} = 0.840 V) exceeded that of the PBDT-Cl:A2-based OSC (V_{oc} = 0.828 V). Moreover, the V_{oc} of PBDT-Cl:A3-based OSC (V_{oc} = 0.840 V) significantly surpassed that of PBDT-Cl:A1-based OSC (V_{oc} = 0.771 V). Such large differences in the V_{oc}s of the OSCs are mainly related to the V_{loss} of the devices,

which is discussed in Section 2.4 below. In other parameters, the J_{sc}s and FFs of PBDT-Cl:A3- based OSCs (J_{sc} = 25.88 mA cm^{-2} and FF = 0.76) and PBDT-Cl:A4-based OSCs (J_{sc} = 26.90 mA cm^{-2} and FF = 0.76) also considerably exceeded those of the PBDT-Cl:A1-based OSCs (J_{sc} = 24.13 mA cm^{-2} and FF = 0.71) and PBDT-Cl:A2-based OSCs (J_{sc} = 25.79 mA cm^{-2} and FF = 0.73), respectively. The maximum EQE of OSCs based on the A2 and A4 SMAs containing IC-F end-groups is close to 91% at 520 nm, which is very high value. In addition, these OSCs demonstrate higher EQE values in 500–800 nm than OSCs based on A1 and A3 SMAs containing IC-Cl end-groups, indicating more efficient light harvesting and photon-to-electron conversion in the visible region. The calculated J_{sc}s of the OSCs based on their EQE spectrum agree well with their measured J_{sc}s within an error of 4%.

2.3. Charge Generation and Recombination

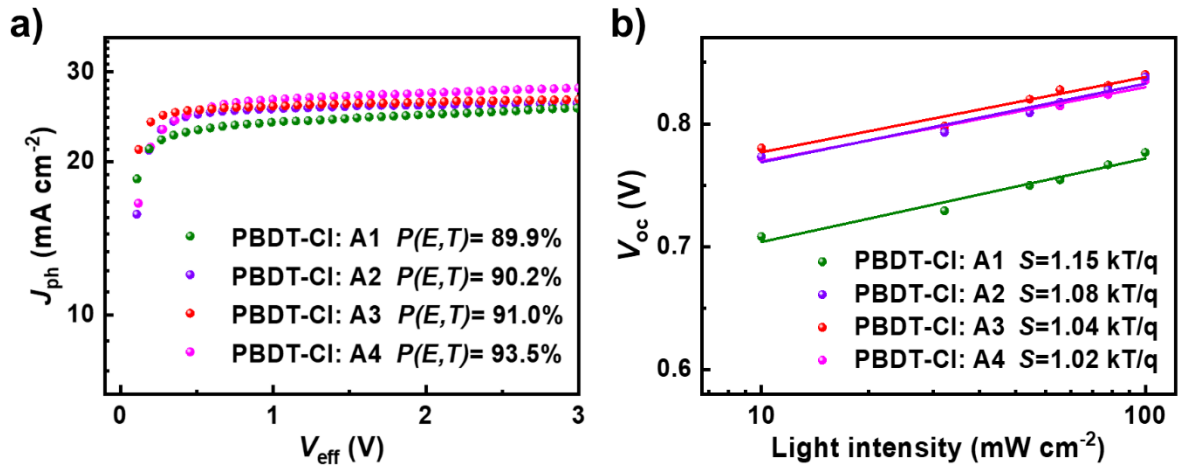

Figure 4. a) J_{ph}–V_{eff} curves of PBDT-Cl:AX (X = 1, 2, 3, or 4)-based OSCs and b) the P_{light}–dependent V_{oc} of the OSCs (from 0.1 to 1 Sun).

To understand the charge generation and recombination properties of PBDT-Cl:AX (X = 1, 2, 3, or 4)-based OSCs, their exciton dissociation probability ($P(E,T)$) and light intensity (P_{light})–dependent V_{oc} were investigated (**Figure 4**). The $P(E,T)$ of each device was calculated by the ratio of its photocurrent density (J_{ph}) under the short-circuit conditions to its saturated J_{ph} value at an effective voltage (V_{eff}) of 3 V.[17] The $P(E,T)$s of the PBDT-Cl:AX–based OSCs slightly increase, in terms of the SMA, in the order A1 (89.9%), A2 (90.2%), A3 (91.0%), and A4 (93.5%) (**Figure 4a**). These results indicate that

the OSCs based on the A3 and A4 SMAs with Ph-Cl side-chains exhibit more efficient exciton dissociation and charge generation than OSCs based on the A1 and A2 SMAs. **Figure 4b** shows the V_{oc}–ln(P) (from 0.1 to 1 Sun) plots of the PBDT-Cl:AX-based OSCs. The slope (S) is expressed in $k_B T q^{-1}$, where k_B is the Boltzmann constant, T is the temperature, and q is the elementary charge.[18] The PBDT-Cl:A4-based OSC showed a smaller S value of 1.02, compared to PBDT-Cl:A2-based OSC (S = 1.08). Similarly, the S value of PBDT-Cl:A3-based OSC (S = 1.04) was lower than that of PBDT-Cl:A1-based OSC (S = 1.15). Interestingly, monomolecular recombination is effectively suppressed in the OSCs based on the A3 and A4 SMAs, resulting in their higher FFs.[19] In addition, the OSCs based on A2 and A4 SMAs (featuring IC-F end-groups) showed less severe recombination properties than the OSCs based on A1 and A3 SMAs (featuring IC-Cl end-groups), respectively, mainly due to the higher μ_es and crystallinity of the SMAs featuring IC-F end-groups.

2.4. Voltage Loss Analysis

Table 3. The overall V_{loss} and the corresponding V_{loss} terms (ΔV_1, ΔV_2, and ΔV_3) of the PBDT-Cl:AX (X = 1, 2, 3, and 4)-based OSCs. All units of measurements are volt [V].

Blend film	E_g^{PV}/q	V_{oc}^{SQ}	V_{oc}^{Rad}	V_{oc}^{PV}	ΔV_1	ΔV_2	ΔV_3	V_{loss}
PBDT-Cl:A1	1.418	1.160	1.123	0.771	0.258	0.037	0.352	0.647
PBDT-Cl:A2	1.432	1.173	1.148	0.828	0.259	0.025	0.320	0.604
PBDT-Cl:A3	1.408	1.151	1.118	0.840	0.257	0.033	0.278	0.568
PBDT-Cl:A4	1.427	1.168	1.152	0.840	0.259	0.016	0.312	0.587

To elucidate the trend in the V_{oc}s of the PBDT-Cl:AX (X = 1, 2, 3, and 4)-based OSCs, we investigated their V_{loss}, which significantly affects their device performance.[4a, 4f, 20] In general, according to the Shockley-Queisser (SQ) theory, V_{loss} consists of three different terms:[21] $V_{loss} = (E_g^{PV}/q - V_{oc}^{SQ}) + (V_{oc}^{SQ} - V_{oc}^{Rad}) + (V_{oc}^{Rad} - V_{oc}^{PV}) = \Delta V_1 + \Delta V_2 + \Delta V_3$, where q, E_g^{PV}, V_{oc}^{SQ}, V_{oc}^{Rad}, and V_{oc}^{PV} are the elementary charge, optical bandgap determined from the derivatives of the EQE spectra (also called photovoltaic bandgap),

maximum voltage by the SQ limit, a voltage in the radiative limit, and photovoltaic V_{oc}, respectively. The three terms (ΔV_1, ΔV_2, and ΔV_3) and their sum (V_{loss}) for each OSC are summarized in **Table 3**. The methods for measuring V_{loss} and detailed calculation process of ΔV_1, ΔV_2, and ΔV_3 are described in the Experimental Section and **Figure S12**. The first term, ΔV_1, is an intrinsically unavoidable factor of the OSCs, which originates from unsatisfying the principle of detailed balance of the solar cells under the illumination of sun.[4a] The ΔV_1 typically has a value of 0.25–0.30 V. The second term, ΔV_2, is caused by the radiative recombination process in solar cells working under the illumination. Lastly, the third term, ΔV_3, represents the non-radiative V_{loss}, which impacts the overall V_{loss} of an OSC most significantly.[20a] This term can be calculated according to the equation $\Delta V_3 = V_{loss} - \Delta V_1 - \Delta V_2$ or from their electroluminescence quantum efficiency (EQE_{EL}) spectra (**Figure S12b** and **Table S4**).[22]

Table 3 shows that the ΔV_1 values of the PBDT-Cl:AX (X = 1, 2, 3, and 4)-based OSCs are similar, in the range of 0.257–0.259 V. The ΔV_2 values of the PBDT-Cl:A3- and PBDT-Cl:A4-based OSCs (0.033 and 0.016 V, respectively), are lower than those of PBDT-

Cl:A1- and PBDT-Cl:A2-based OSCs, respectively (0.037 and 0.025 V). This result indicates that the A3 and A4 SMAs with Ph-Cl side-chains have lower energy offsets, compared to those of the A1 and A2 SMAs with Ph-H side-chains.[4a] Importantly, significant differences were observed in the ΔV_3 values of the blends. In particular, the ΔV_3 value of the PBDT-Cl:A3–based OSC (0.278 V) is much lower than that of the PBDT-Cl:A1–based OSC (0.352 V), suggesting that the introduction of Cl atoms into the inner side-chains of the SMAs significantly reduces non-radiative V_{loss}. Similarly, the ΔV_3 value of the PBDT-Cl:A4-based OSC is lower than that of the PBDT-Cl:A2–based OSC. As non-radiative V_{loss} can be closely related to the energetic interactions at the P_Ds/SMAs interfaces,[9e] we investigated the morphologies of PBDT-Cl:AX (X = 1, 2, 3, and 4) blend films.

2.5. Crystalline Characteristics and Charge Mobility

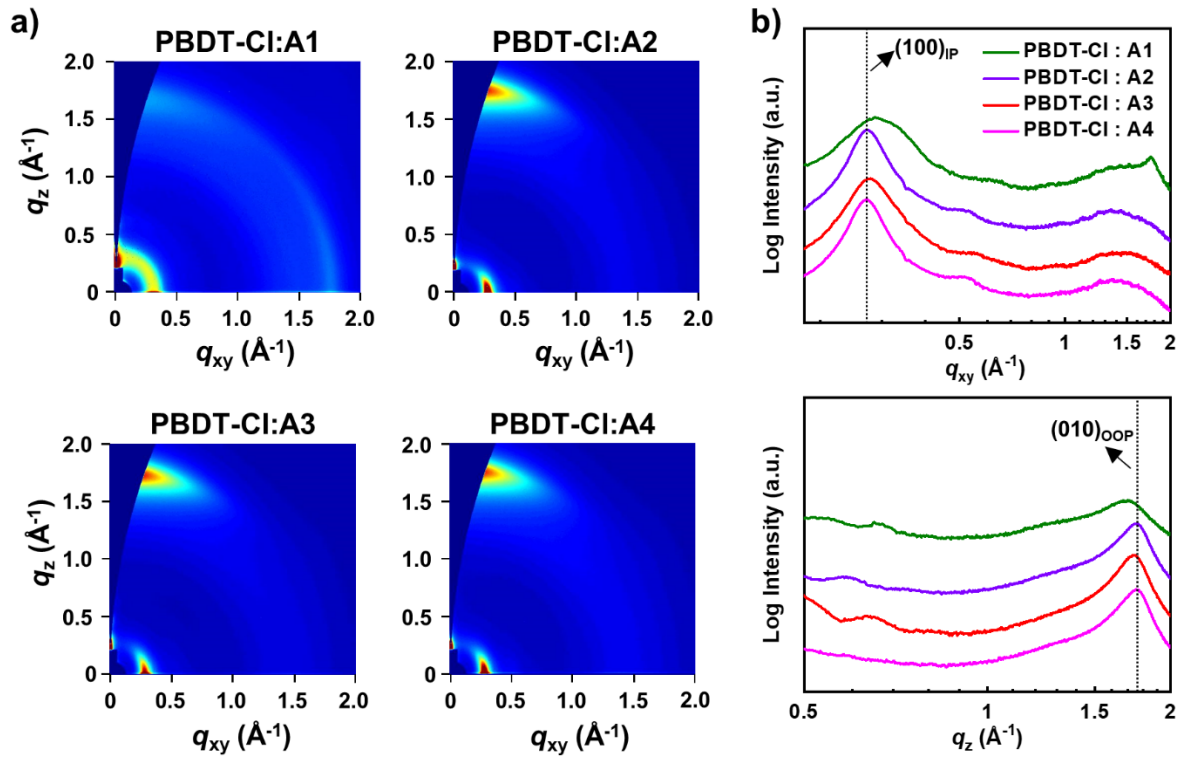

Figure 5. a) 2D GIXS images of PBDT-Cl:AX (X = 1, 2, 3, and 4) blend films and b) corresponding line-cut profiles along the IP (q_{xy}) and OOP (q_z) directions.

Table 4. Charge mobilities of the PBDT-Cl:AX (X = 1, 2, 3, and 4) blend films.

Blend Film	μ_e [cm^2 V^{-1} s^{-1}]	μ_h [cm^2 V^{-1} s^{-1}]	μ_h/μ_e

PBDT-Cl:A1	1.2×10^{-4}	2.1×10^{-4}	1.8
PBDT-Cl:A2	1.4×10^{-4}	2.4×10^{-4}	1.7
PBDT-Cl:A3	1.7×10^{-4}	2.3×10^{-4}	1.4
PBDT-Cl:A4	1.9×10^{-4}	2.2×10^{-4}	1.2

To understand the effect of the halogens in the side-chains and IC end-groups of SMAs on the molecular packing structures and crystalline properties in their pristine and blend films, we conducted grazing incidence wide-angle X-ray scattering (GIXS) measurement (**Figure 5** and **Figure S13**). As shown in **Figure S13**, A1, A2, A3, and A4 pristine films showed largely different packing structures depending on their degree of halogenation. In the case of SMAs featuring IC-Cl end-groups, the packing structure of the A1 film showed an edge-on orientation, while that of the A3 film exhibited a slanted orientation, forming a dihedral angle (χ) of 48.5°. In the case of SMAs featuring IC-F end-groups, the packing structure of the A2 film showed a slanted orientation (χ = 17.5°), whereas that of the A4 film exhibited a face-on orientation, which is favorable for vertical

charge transport.[23] These results indicate that the chlorination of the terminal benzene rings of the inner side-chains of the SMAs can promote the face-on orientation from A1 to A3 and A2 to A4. Also, the chlorination of the side-chains resulted in the enhanced crystallinity of the SMAs.

The 2D GIXS images of each blend film are presented in **Figure 5a**, and their line-cut profiles along the in-plane (IP) and out-of-plane (OOP) directions are shown in **Figure 5b**. Evidently, it was found that the halogenation on the IC end-groups or side-chains of SMAs significantly affects the overall molecular packing orientations of resulting blend films. For example, edge-on packing orientation of A1 SMA was well preserved in its own crystal regions of the blend film with the face-on-oriented PBDT-Cl P_D, showing mixed face-on and edge-on packing orientations. This bimodal orientation can cause increased charge recombination and unfavorable charge dissociation/transport at the D/A interfaces, thereby increasing the non-radiative V_{loss} of a resulting OSC.[4f, 20a] On the other hand, A2, A3, and A4-based blend films showed predominantly face-on orientations, as indicated by distinct $(010)_{OOP}$ and $(100)_{IP}$ scattering peaks in their line-cut

profiles.[24] To quantitatively compare the crystallinity and packing structures of the four blend films, their crystal coherence lengths (L_cs) were determined from the $(100)_{IP}$ peaks using the Scherrer equation,[25] and their π–π stacking distances ($d_{\pi-\pi}$) were calculated from the $(010)_{OOP}$ peaks using $d=2\pi q^{-1}$,[26] as shown in **Table S5**. In the case of the blend films based on SMAs featuring IC-F end-groups, the L_c (125.9 Å) and $d_{\pi-\pi}$ (3.59 Å) of the PBDT-Cl:A4 blend film were greater than and less than, respectively, those of the PBDT-Cl:A2 blend film (L_c = 102.9 Å and $d_{\pi-\pi}$ = 3.61 Å). Similarly, in the case of the blend films based on SMAs featuring IC-Cl end-groups, the L_c (99.2 Å) and $d_{\pi-\pi}$ (3.63 Å) of the PBDT-Cl:A3 blend film were greater than and less than, respectively, those of the PBDT-Cl:A1 blend film (L_c = 53.0 Å and $d_{\pi-\pi}$ = 3.77 Å). These results suggest that the Cl atoms in the Ph-Cl side-chains of SMAs play a key role in promoting tight molecular packing and enhancing the crystallinity of the PBDT-Cl:AX blend films (**Table S5**). In particular, the PBDT-Cl:A4 blend film showed the highest crystallinity, which is consistent with the superior PCE of the corresponding OSC.

To understand the electrical properties of the blend films, the charge mobilities of each blend were evaluated using the SCLC method. The PBDT-Cl:A3 (μ_e = 1.7 × 10^{-4} cm^2 V^{-1} S^{-1}) and PBDT-Cl:A4 (μ_e = 1.9 × 10^{-4} cm^2 V^{-1} S^{-1}) blend films showed higher μ_es than those of the PBDT-Cl:A1 (μ_e = 1.2 × 10^{-4} cm^2 V^{-1} S^{-1}) and PBDT-Cl:A2 (μ_e = 1.4 × 10^{-4} cm^2 V^{-1} S^{-1}) blend films, respectively (**Table 4**). In addition, the PBDT-Cl:A3 and PBDT-Cl:A4 blend films exhibit more balanced hole and electron mobilities (μ_h/μ_e), 1.4 and 1.2, respectively, than the PBDT-Cl:A1 (1.8) and PBDT-Cl:A2 (1.7) blend films, which contribute to suppressed charge recombination and a higher FF.[4f, 27]

2.6. Morphological Properties of Blend Films

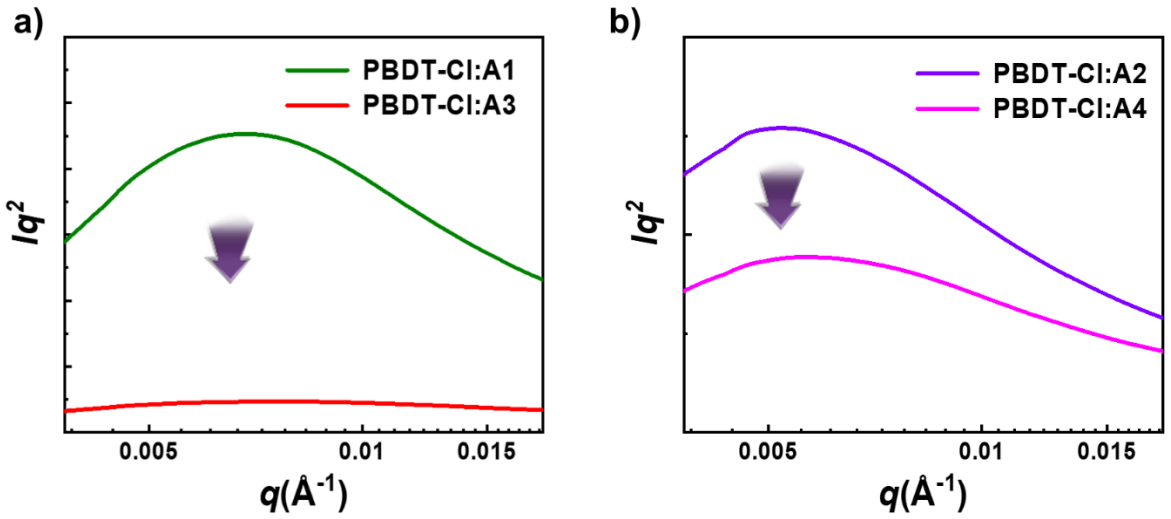

Figure 6. RSoXS profiles of a) PBDT-Cl:A1 and PBDT-Cl:A3, and b) PBDT-Cl:A2 and PBDT-Cl:A4 blend films.

To better understand the effect of the chlorination of the side-chains in the SMAs on the blend morphologies such as phase separation behaviors, the resonant soft X-ray scattering (RSoXS) measurement was performed. (**Figure 6**). For a distinct contrast between the P_D and SMAs, the RSoXS profiles were obtained from a beam energy of 284.4 eV.[28] The domain size and purity of the blend films were calculated based on their RSoXS profiles (Experimental Section and **Table S6**).[29] Interestingly, the PBDT-Cl:A3

blend film (40.6 nm) showed a smaller domain size than that of the PBDT-Cl:A1 blend film (45.6 nm). Also, PBDT-Cl:A4 blend film (56.2 nm) also exhibited smaller domain size than that of the PBDT-Cl:A2 blend film (60.4 nm). Importantly, the domain purity of the PBDT-Cl:A3 blend film (relative domain purity = 0.34) was significantly lower than that of the PBDT-Cl:A1 blend film. Similarly, the PBDT-Cl:A4 blend film showed a smaller relative domain purity of 0.79 compared to the PBDT-Cl:A2 blend. These results indicate that the blend films based on SMAs featuring chlorinated side-chains, Ph-Cl, can form better-intermixed domains than blend films based on SMAs featuring non-chlorinated side-chains. Such well-intermixed blend morphologies contributed to suppressed charge recombination and enhanced charge generation, allowing the OSC devices to have higher J_{sc} and FF values.[19, 30]

Table 5. Summary of the contact angles and surface tension of PBDT-Cl, A1, A2, A3, and A4 films, and the interfacial tension between PBDT-Cl P_D and SMAs.

Material	Contact Angle [deg]	Surface	Blend Systems	$\gamma^{D-A\ a)}$	[mN

	water	Glycerol	Tension [mN m^{-1}]		m^{-1}]
PBDT-Cl	99.5	86.8	23.26	–	–
A1	97.2	81.1	27.31	PBDT-Cl:A1	0.67
A2	97.1	82.0	26.39	PBDT-Cl:A2	0.33
A3	97.9	83.0	25.85	PBDT-Cl:A3	0.28
A4	97.6	83.4	25.36	PBDT-Cl:A4	0.13

[a] The interfacial tension between the PBDT-Cl P_D and SMAs.

To elucidate the differences in blend intermixing, we calculated the interfacial tension ($\gamma^{D\text{-}A}$) between the PBDT-Cl P_D and SMAs using the Wu model.[31] The water and glycerol contact angles of each material were measured (**Table 5** and **Figure S14**). The detailed calculation process, related equations, and resulting dispersive (γ^d) and polar (γ^p) components of each material are described in the Experimental Section and **Tables S7**–**S8**. Interestingly, the $\gamma^{D\text{-}A}$ values of PBDT-Cl:A3 and PBDT-Cl:A4 blends (based on SMAs

featuring Ph-Cl side-chains) of 0.28 and 0.13 mN m^{-1}, respectively, are lower than those of PBDT-Cl:A1 (0.67 mN m^{-1}) and PBDT-Cl:A2 (0.33 mN m^{-1}) blends (based on SMAs featuring Ph-H side-chain) (**Table 5**). A low $\gamma^{D\text{-}A}$ is indicative of high interfacial compatibility between the P_D and SMA, which can induce well-intermixed domains with large D/A interfacial areas by suppressing severe phase separation.[32] This trend is consistent well with the results of the RSoXS measurements. In addition, we compared the thermal stabilities of the PBDT-Cl:AX (X= 1, 2, 3, or 4)-based OSCs at 120°C. The normalized PCE_{avg}s of the four blends and their photovoltaic parameters as a function of annealing time are presented in **Figure S15** and **Table S9**. Interestingly, A1 and A2 SMAs (with non-chlorinated side-chains)-based OSCs retained 75% and 83% of its initial PCE_{avg} after annealing at 120°C for 100 hr, respectively. In contrast, A3 and A4 SMAs (with chlorinated side-chains)-based devices demonstrated superior thermal stabilities, maintaining more than 92% of its initial PCE under the same condition. This result indicates that improved interfacial compatibility between P_D and SMA can better stabilize

the phase-separated nanodomains against thermal stress, preventing severe aggregations.[32a, 33]

Based on our analyses (GIXS, RSoXS, and $\gamma^{D\text{-}A}$ results), we conclude that the high ΔV_3 value of the PBDT-Cl:A1-based OSC is mainly caused by excessive domain purity and the undesirable bimodal packing orientations. Conversely, in the A3-based blend, the ΔV_3 value was effectively suppressed due to the increased miscibility between the A3 SMA (with Ph-Cl side-chain) and the PBDT-Cl P_D, and the favorable face-on orientation of the blend films. In the case of A2 and A4 SMAs, although the packing structures of PBDT-Cl:A2 and PBDT-Cl:A4 blend films showed similar face-on orientations, the PBDT-Cl:A4 blend film achieved better-intermixed domains and a lower ΔV_3 value than the PBDT-Cl:A2 blend film. Therefore, PBDT-Cl:A4 blend film with its high μ_e and optimal D/A blend morphology afforded the OSC with the highest PCE of 17.19%. The improved properties of the PBDT-Cl:A4 blend film were achieved synergistically through the selective halogenation on both the IC end-groups and inner side-chains of the SMA.

3. Conclusion

In summary, we investigated the effects of the selective halogenation of SMAs on the blend morphology, V_{loss} and photovoltaic performance. For a systematic study, we synthesized four SMAs (*i.e.*, A1, A2, A3, and A4) with different halogenations at two different positions of inner side-chains and IC end-groups. It was found that appropriate halogenations on both the inner side-chains and IC end-groups of the SMA impact the pristine and blend morphologies; 1) SMAs featuring IC-F end-groups exhibit more enhanced molecular ordering and thin-film crystallinity than SMAs having IC-Cl end-groups, indicating the importance of the selection of a suitable halogen atom in IC end-groups. 2) The chlorination on the inner side-chains of SMA can promote its intermixing with P_D and induce a favorable face-on packing orientation of the SMA, thus reducing the energetic disorder at the D/A interface and enhancing the PCE. As a result, the OSC based on A4 SMA featuring both IC-F end-groups and Ph-Cl side-chains achieved the highest PCE of 17.19%, enabled by the high crystallinity, improved charge mobility, and suppressed non-radiative V_{loss}. Our study demonstrates the utility of the halogenation at

the selective position of SMAs in the optimization of the blend morphology and photovoltaic performance of OSCs.

Supporting Information

Materials and synthesis, general characterizations, calculation for V_{loss}, and fabrication of OSCs are included in the Supporting Information. Supporting Information is available from the Wiley Online Library or from the author.

Conflicts of interest

There are no conflicts to declare.

Acknowledgements

G.-U K., C. S., D. L., and G.-S. C. contributed equally to this work. This work was supported by National Research Foundation of Korea (NRF) Grant of the Korean Government (2020R1A4A1018516, 2021R1A2B5B03086367, and 2019R1A6A1A11053838).

The experiment at the Advanced Light Source was supported by a DOE office of Science User Facility under contract no. DE-AC02-05CH11231.

References

[1] a) T. Kim, J.-H. Kim, T. E. Kang, C. Lee, H. Kang, M. Shin, C. Wang, B. Ma, U. Jeong, T.-S. Kim, B. J. Kim, *Nat. Commun.* **2015**, *6*, 8547; b) M. Kaltenbrunner, M. S. White, E. D. Głowacki, T. Sekitani, T. Someya, N. S. Sariciftci, S. Bauer, *Nat. Commun.* **2012**, *3*, 770; c) J. Noh, G.-U Kim, S. Han, S. J. Oh, Y. Jeon, D. Jeong, S. W. Kim, T.-S. Kim, B. J. Kim, J.-Y. Lee, *ACS Energy Lett.* **2021**, *6*, 2512; d) M. Riede, D. Spoltore, K. Leo, *Adv. Energy Mater.* **2021**, *11*, 2002653; e) C. Lee, S. Lee, G.-U Kim, W. Lee, B. J. Kim, *Chem. Rev.* **2019**, *119*, 8028; f) S. Chen, S. Jung, H. J. Cho, N.-H. Kim, S. Jung, J. Xu, J. Oh, Y. Cho, H. Kim, B. Lee, Y. An, C. Zhang, M. Xiao, H. Ki, Z.-G. Zhang, J.-Y. Kim, Y. Li, H. Park, C. Yang, *Angew. Chem., Int. Ed.* **2018**, *57*, 13277.

[2] a) Y. Cui, Y. Xu, H. Yao, P. Bi, L. Hong, J. Zhang, Y. Zu, T. Zhang, J. Qin, J. Ren, Z. Chen, C. He, X. Hao, Z. Wei, J. Hou, *Adv. Mater.* **2021**, *33*, 2102420; b) J. Yuan, Y. Zhang, L. Zhou, G. Zhang, H.-L. Yip, T.-K. Lau, X. Lu, C. Zhu, H. Peng, P. A. Johnson, M. Leclerc, Y. Cao, J. Ulanski, Y. Li, Y. Zou, *Joule* **2019**, *3*, 1140; c) Y. Cui, H. Yao, L. Hong, T. Zhang, Y. Tang, B. Lin, K. Xian, B. Gao, C. An, P. Bi, W. Ma, J. Hou, *Natl. Sci. Rev.* **2020**, *7*, 1239; d) Y. Cui, H. Yao, J. Zhang, K. Xian, T. Zhang, L. Hong, Y. Wang, Y. Xu, K. Ma, C. An, C. He, Z. Wei, F. Gao, J. Hou, *Adv. Mater.* **2020**, *32*, 1908205; e) S. Lee, D. Jeong, C. Kim, C. Lee, H. Kang, H. Y. Woo, B. J. Kim, *ACS Nano* **2020**, *14*, 14493.

[3] S. Li, C.-Z. Li, M. Shi, H. Chen, *ACS Energy Lett.* **2020**, *5*, 1554.

[4] a) J. Wang, H. Yao, Y. Xu, L. Ma, J. Hou, *Mater. Chem. Front.* **2021**, *5*, 709; b) P. Cheng, G. Li, X. Zhan, Y. Yang, *Nat. Photonics* **2018**, *12*, 131; c) J. Zhang, H. S. Tan, X. Guo, A. Facchetti, H. Yan, *Nat. Energy* **2018**, *3*, 720; d) K. Kawashima, Y. Tamai, H. Ohkita, I. Osaka, K. Takimiya, *Nat. Commun.* **2015**, *6*, 10085; e) F.-Y. Cao, C.-C.

Tseng, F.-Y. Lin, Y. Chen, H. Yan, Y.-J. Cheng, *Chem. Mater.* **2017**, *29*, 10045; f) G.-U Kim, C. Sun, J. S. Park, H. G. Lee, D. Lee, J.-W. Lee, H. J. Kim, S. Cho, Y.-H. Kim, S.-K. Kwon, B. J. Kim, *Adv. Funct. Mater.* **2021**, *31*, 2100870; g) J.-W. Lee, C. Sun, D. J. Kim, M. Y. Ha, D. Han, J. S. Park, C. Wang, W. B. Lee, S.-K. Kwon, T.-S. Kim, Y.-H. Kim, B. J. Kim, *ACS Nano* **2021**, *15*, 19970; h) N. B. Kolhe, D. K. Tran, H. Lee, D. Kuzuhara, N. Yoshimoto, T. Koganezawa, S. A. Jenekhe, *ACS Energy Lett.* **2019**, *4*, 1162.

[5] a) T. Liu, Y. Zhang, Y. Shao, R. Ma, Z. Luo, Y. Xiao, T. Yang, X. Lu, Z. Yuan, H. Yan, Y. Chen, Y. Li, *Adv. Funct. Mater.* **2020**, *30*, 2000456; b) Z. Luo, R. Ma, Z. Chen, Y. Xiao, G. Zhang, T. Liu, R. Sun, Q. Zhan, Y. Zou, C. Zhong, Y. Chen, H. Sun, G. Chai, K. Chen, X. Guo, J. Min, X. Lu, C. Yang, H. Yan, *Adv. Energy Mater.* **2020**, *10*, 2002649; c) H. Sun, B. Liu, Y. Ma, J.-W. Lee, J. Yang, J. Wang, Y. Li, B. Li, K. Feng, Y. Shi, B. Zhang, D. Han, H. Meng, L. Niu, B. J. Kim, Q. Zheng, X. Guo, *Adv. Mater.* **2021**, *33*, 2102635; d) R. Zhao, N. Wang, Y. Yu, J. Liu, *Chem. Mater.* **2020**, *32*, 1308; e) D. Li, C. Guo, X. Zhang, B. Du, C. Yu, P. Wang, S. Cheng, L. Wang, J. Cai, H. Wang, D. Liu, H. Yao, Y. Sun, J. Hou, T. Wang, *Sci. China Chem.* **2021**, *65*, 373; f) Y. Cui, H. Yao, J. Zhang, T. Zhang, Y. Wang, L. Hong, K. Xian, B. Xu, S. Zhang, J. Peng, Z. Wei, F. Gao, J. Hou, *Nat. Commun.* **2019**, *10*, 2515; g) H. Lai, Q. Zhao, Z. Chen, H. Chen, P. Chao, Y. Zhu, Y. Lang, N. Zhen, D. Mo, Y. Zhang, F. He, *Joule* **2020**, *4*, 688; h) C. Kim, S. Chen, J. S. Park, G.-U Kim, H. Kang, S. Lee, T. N.-L. Phan, S.-K. Kwon, Y.-H. Kim, B. J. Kim, *J. Mater. Chem. A* **2021**, *9*, 24622.

[6] a) P. Tan, L. Liu, Z.-Y. Chen, H. Lai, Y. Zhu, H. Chen, N. Zheng, Y. Zhang, F. He, *Adv. Funct. Mater.* **2021**, *31*, 2106524; b) Z. Genene, J.-W. Lee, S.-W. Lee, Q. Chen, Z. Tan, B. A. Abdulahi, D. Yu, T.-S. Kim, B. J. Kim, E. Wang, *Adv. Mater.* **2021**, 2107361; c) C. Sun, J.-W. Lee, S. Seo, S. Lee, C. Wang, H. Li, Z. Tan, S.-K. Kwon, B.

J. Kim, Y.-H. Kim, *Adv. Energy Mater.* **2022**, *12*, 2103239; d) S. Seo, C. Sun, J.-W. Lee, S. Lee, D. Lee, C. Wang, T. N.-L. Phan, G.-U Kim, S. Cho, Y.-H. Kim, B. J. Kim, *Adv. Funct. Mater.* **2021**, 2108508; e) B. Liu, H. Sun, J.-W. Lee, J. Yang, J. Wang, Y. Li, B. Li, M. Xu, Q. Liao, W. Zhang, D. Han, L. Niu, H. Meng, B. J. Kim, X. Guo, *Energy Environ. Sci.* **2021**, *14*, 4499; f) L. Zhang, T. Jia, L. Pan, B. Wu, Z. Wang, K. Gao, F. Liu, C. Duan, F. Huang, Y. Cao, *Sci. China Chem.* **2021**, *64*, 408.

[7] a) H. Wang, T. Liu, J. Zhou, D. Mo, L. Han, H. Lai, H. Chen, N. Zheng, Y. Zhu, Z. Xie, F. He, *Adv. Sci.* **2020**, *7*, 1903784; b) N. Bauer, Q. Zhang, J. J. Rech, S. Dai, Z. Peng, H. Ade, J. Wang, X. Zhan, W. You, *Nano Res.* **2019**, *12*, 2400; c) Q. Zhao, J. Qu, F. He, *Adv. Sci.* **2020**, *7*, 2000509; d) C. Yao, J. Zhao, Y. Zhu, B. Liu, C. Yan, D. F. Perepichka, H. Meng, *ACS Appl. Mater. Interfaces* **2020**, *12*, 11543; e) A. Wadsworth, M. Moser, A. Marks, M. S. Little, N. Gasparini, C. J. Brabec, D. Baran, I. McCulloch, *Chem. Soc. Rev.* **2019**, *48*, 1596; f) H. Wang, F. He, *Synlett* **2021**, *32*, 1297; g) H. Chen, Z. Hu, H. Wang, L. Liu, P. Chao, J. Qu, W. Chen, A. Liu, F. He, *Joule* **2018**, *2*, 1623; h) H. Chen, T. Zhao, L. Li, P. Tan, H. Lai, Y. Zhu, X. Lai, L. Han, N. Zheng, L. Guo, F. He, *Adv. Mater.* **2021**, *33*, 2102778; i) G. Li, X. Zhang, L. O. Jones, J. M. Alzola, S. Mukherjee, L.-w. Feng, W. Zhu, C. L. Stern, W. Huang, J. Yu, V. K. Sangwan, D. M. DeLongchamp, K. L. Kohlstedt, M. R. Wasielewski, M. C. Hersam, G. C. Schatz, A. Facchetti, T. J. Marks, *J. Am. Chem. Soc.* **2021**, *143*, 6123; j) G. Li, L.-W. Feng, S. Mukherjee, L. O. Jones, R. M. Jacobberger, W. Huang, R. M. Young, R. M. Pankow, W. Zhu, N. Lu, K. L. Kohlstedt, V. K. Sangwan, M. R. Wasielewski, M. C. Hersam, G. C. Schatz, D. M. DeLongchamp, A. Facchetti, T. J. Marks, *Energy & Environ. Sci.* **2022**, *15*, 645.

[8] X. Zhang, G. Li, S. Mukherjee, W. Huang, D. Zheng, L.-W. Feng, Y. Chen, J. Wu, V. K. Sangwan, M. C. Hersam, D. M. DeLongchamp, J. Yu, A. Facchetti, T. J. Marks, *Adv. Energy Mater.* **2022**, *12*, 2102172.

[9] a) J. Yuan, T. Huang, P. Cheng, Y. Zou, H. Zhang, J. L. Yang, S.-Y. Chang, Z. Zhang, W. Huang, R. Wang, D. Meng, F. Gao, Y. Yang, *Nat. Commun.* **2019**, *10*, 570; b) S. Liu, J. Yuan, W. Deng, M. Luo, Y. Xie, Q. Liang, Y. Zou, Z. He, H. Wu, Y. Cao, *Nat. Photonics* **2020**, *14*, 300; c) T. Saito, S.-i. Natsuda, K. Imakita, Y. Tamai, H. Ohkita, *Sol. RRL* **2020**, *4*, 2000255; d) K. D. Rosenthal, M. P. Hughes, B. R. Luginbuhl, N. A. Ran, A. Karki, S.-J. Ko, H. Hu, M. Wang, H. Ade, T.-Q. Nguyen, *Adv. Energy Mater.* **2019**, *9*, 1901077; e) J. Yuan, H. Zhang, R. Zhang, Y. Wang, J. Hou, M. Leclerc, X. Zhan, F. Huang, F. Gao, Y. Zou, Y. Li, *Chem* **2020**, *6*, 2147.

[10] S. Chen, Y. Liu, L. Zhang, P. C. Y. Chow, Z. Wang, G. Zhang, W. Ma, H. Yan, *J. Am. Chem. Soc.* **2017**, *139*, 6298.

[11] N. A. Ran, S. Roland, J. A. Love, V. Savikhin, C. J. Takacs, Y.-T. Fu, H. Li, V. Coropceanu, X. Liu, J.-L. Brédas, G. C. Bazan, M. F. Toney, D. Neher, T.-Q. Nguyen, *Nat. Commun.* **2017**, *8*, 79.

[12] J. S. Park, G.-U Kim, D. Lee, S. Lee, B. Ma, S. Cho, B. J. Kim, *Adv. Funct. Mater.* **2020**, *30*, 2005787.

[13] T.-W. Chen, K.-L. Peng, Y.-W. Lin, Y.-J. Su, K.-J. Ma, L. Hong, C.-C. Chang, J. Hou, C.-S. Hsu, *J. Mater. Chem. A* **2020**, *8*, 1131.

[14] Z. Chiguvare, V. Dyakonov, *Phys. Rev. B* **2004**, *70*, 235207.

[15] D. Baran, R. S. Ashraf, D. A. Hanifi, M. Abdelsamie, N. Gasparini, J. A. Röhr, S. Holliday, A. Wadsworth, S. Lockett, M. Neophytou, C. J. M. Emmott, J. Nelson, C. J. Brabec, A. Amassian, A. Salleo, T. Kirchartz, J. R. Durrant, I. McCulloch, *Nat. Mater.* **2017**, *16*, 363.

[16] J. Yao, B. Qiu, Z.-G. Zhang, L. Xue, R. Wang, C. Zhang, S. Chen, Q. Zhou, C. Sun, C. Yang, M. Xiao, L. Meng, Y. Li, *Nat. Commun.* **2020**, *11*, 2726.

[17] P. W. M. Blom, V. D. Mihailetchi, L. J. A. Koster, D. E. Markov, *Adv. Mater.* **2007**, *19*, 1551.

[18] S. R. Cowan, A. Roy, A. J. Heeger, *Phys. Rev. B* **2010**, *82*, 245207.

[19] J.-W. Lee, D. Jeong, D. J. Kim, T. N.-L. Phan, J. S. Park, T.-S. Kim, B. J. Kim, *Energy Environ. Sci.* **2021**, 14, 4067.

[20] a) S. M. Menke, N. A. Ran, G. C. Bazan, R. H. Friend, *Joule* **2018**, *2*, 25; b) X.-K. Chen, D. Qian, Y. Wang, T. Kirchartz, W. Tress, H. Yao, J. Yuan, M. Hülsbeck, M. Zhang, Y. Zou, Y. Sun, Y. Li, J. Hou, O. Inganäs, V. Coropceanu, J.-L. Bredas, F. Gao, *Nat. Energy* **2021**, *6*, 799; c) J. Liu, S. Chen, D. Qian, B. Gautam, G. Yang, J. Zhao, J. Bergqvist, F. Zhang, W. Ma, H. Ade, O. Inganäs, K. Gundogdu, F. Gao, H. Yan, *Nat. Energy* **2016**, *1*, 16089; d) P. Malhotra, S. Biswas, F.-C. Chen, G. D. Sharma, *Sol. Energy* **2021**, *228*, 175; e) Q. Fan, Q. An, Y. Lin, Y. Xia, Q. Li, M. Zhang, W. Su, W. Peng, C. Zhang, F. Liu, L. Hou, W. Zhu, D. Yu, M. Xiao, E. Moons, F. Zhang, T. D. Anthopoulos, O. Inganäs, E. Wang, *Energy Environ. Sci.* **2020**, *13*, 5017.

[21] W. Shockley, H. J. Queisser, *J. Appl. Phys.* **1961**, *32*, 510.

[22] a) T. Kirchartz, U. Rau, *Phys. Stat. Sol. (a)* **2008**, *205*, 2737; b) B. Fan, F. Lin, J. Oh, H. Fu, W. Gao, Q. Fan, Z. Zhu, W. J. Li, N. Li, L. Ying, F. Huang, C. Yang, A. K.-Y. Jen, *Adv. Energy Mater.* **2021**, *11*, 2101768.

[23] J. Jung, W. Lee, C. Lee, H. Ahn, B. J. Kim, *Adv. Energy Mater.* **2016**, *6*, 1600504.

[24] J. Rivnay, R. Steyrleuthner, L. H. Jimison, A. Casadei, Z. Chen, M. F. Toney, A. Facchetti, D. Neher, A. Salleo, *Macromolecules* **2011**, *44*, 5246.

[25] D. M. Smilgies, *J. Appl. Cryst.* **2009**, *42*, 1030.

[26] J. Rivnay, S. C. Mannsfeld, C. E. Miller, A. Salleo, M. F. Toney, *Chem. Rev.* **2012**, *112*, 5488.

[27] Y. Ma, D. Cai, S. Wan, P. Yin, P. Wang, W. Lin, Q. Zheng, *Natl. Sci. Rev.* **2020**, *7*, 1886.

[28] C. Lee, T. Giridhar, J. Choi, S. Kim, Y. Kim, T. Kim, W. Lee, H.-H. Cho, C. Wang, H. Ade, B. J. Kim, *Chem. Mater.* **2017**, *29*, 9407.

[29] H. Hu, Y. Li, J. Zhang, Z. Peng, L.-k. Ma, J. Xin, J. Huang, T. Ma, K. Jiang, G. Zhang, W. Ma, H. Ade, H. Yan, *Adv. Energy Mater.* **2018**, *8*, 1800234.

[30] a) S. Mukherjee, C. M. Proctor, G. C. Bazan, T.-Q. Nguyen, H. Ade, *Adv. Energy Mater.* **2015**, *5*, 1500877; b) H.-H. Cho, S. Kim, T. Kim, V. G. Sree, S.-H. Jin, F. S. Kim, B. J. Kim, *Adv. Energy Mater.* **2018**, *8*, 1701436.

[31] a) S. Wu, *J. Adhes.* **1973**, *5*, 39; b) K.-H. Kim, H. Kang, H. J. Kim, P. S. Kim, S. C. Yoon, B. J. Kim, *Chem. Mater.* **2012**, *24*, 2373; c) H. Kang, K.-H. Kim, J. Choi, C. Lee, B. J. Kim, *ACS Macro Lett.* **2014**, *3*, 1009.

[32] a) J.-W. Lee, C. Sun, B. S. Ma, H. J. Kim, C. Wang, J. M. Ryu, C. Lim, T.-S. Kim, Y.-H. Kim, S.-K. Kwon, B. J. Kim, *Adv. Energy Mater.* **2021**, *11*, 2003367; b) L. Zhu, M. Zhang, W. Zhong, S. Leng, G. Zhou, Y. Zou, X. Su, H. Ding, P. Gu, F. Liu, Y. Zhang, *Energy Environ. Sci.* **2021**, *14*, 4341.

[33] a) C. Zhang, T. Heumueller, S. Leon, W. Gruber, K. Burlafinger, X. Tang, J. D. Perea, I. Wabra, A. Hirsch, T. Unruh, N. Li, C. J. Brabec, *Energy & Environ. Sci.* **2019**, *12*, 1078; b) J. B. Kim, K. Allen, S. J. Oh, S. Lee, M. F. Toney, Y. S. Kim, C. R. Kagan, C. Nuckolls, Y. L. Loo, *Chem. Mater.* **2010**, *22*, 5762.

TOC

We describe the impacts of sequential halogenation in selective positions of small molecule acceptors (SMAs) on the blend morphology, voltage loss, and photovoltaic performances. As a result, the A4-based organic solar cells exhibit the highest power conversion efficiency of 17.2%, attributed to the optimized blend morphology and reduced voltage loss.